

RTX Positioning: The Next Generation of cm-accurate Real-Time GNSS Positioning

Rodrigo Leandro, Herbert Landau, Markus Nitschke, Markus Glocker, Stephan Seeger, Xiaoming Chen, Alois Deking, Mohamed BenTahar, Feipeng Zhang, Kendall Ferguson, Ralf Stolz, Nick Talbot, Gang Lu, Timo Allison, Markus Brandl, Victor Gomez, Wei Cao, Adrian Kipka
Trimble Terrasat GmbH, Germany

ABSTRACT

The first commercial GPS Real-time Kinematic (RTK) positioning products were released in 1993. Since then RTK technology has found its way into a wide variety of application areas and markets including Survey, Machine Control, and Precision Farming. Current RTK systems provide cm-accurate positioning typically with initialization times of seconds. However, one of the main limitations of RTK positioning is the need of having nearby infra-structure. This infra-structure normally includes a single base station and radio link, or in the case of network RTK, several reference stations with internet connections, a central processing center and communication links to users. In single-base, or network RTK, the distances between reference stations and the rover receiver are typically limited to 100 km.

During the last decade several researchers have advocated Precise Point Positioning (PPP) techniques as an alternative to reference station-based RTK. With the PPP technique the GNSS positioning is performed using precise satellite orbit and clock information, rather than corrections from one or more reference stations. The published PPP solutions typically provide position accuracies of better than 10 cm horizontally. The major drawback of PPP techniques is the relatively slow convergence time required to achieve kinematic position accuracies of 10 cm or better. PPP convergence times are typically on the order of several tens of minutes, but occasionally the convergence may take a couple of hours depending on satellite geometry and prevailing atmospheric conditions. Long initialization time is a limiting factor in considering PPP as a practical solution for positioning systems that rely on productivity and availability. Nevertheless, PPP techniques are very appealing from a ground infrastructure and operational coverage area perspective, since precise positioning could be potentially performed in any place where satellite correction data is available.

For several years, efforts have been made by numerous organizations in attempting to improve the productivity of PPP-like solutions. Simultaneously, efforts have been made to improve network RTK performance with sparsely located reference stations. Until now there has not been a workable solution for either approach. Commercial success of the published PPP solutions for

high-accuracy applications has been limited by the low productivity compared to established RTK methods.

In this paper we present a technology that brings together the advantages of both types of solutions, i.e., positioning techniques that do not require local reference stations while providing the productivity of RTK positioning. This means coupling the high productivity and accuracy of reference station-based RTK systems with the extended coverage area of solutions based on global satellite corrections. The outcome of this new technology is the positioning service CENTERPOINT RTX™, which provides real-time cm-level accuracy without the direct use of a reference station infrastructure, that is suitable for many GNSS market segments. Furthermore, the RTX solution is applicable to multi-GNSS constellations. The new technology involves innovations in RTK network processing, as well as advancements in the rover RTK positioning algorithms.

INTRODUCTION

The RTX (**R**eal **T**ime **e**Xtended) positioning solution is the technology resulting from the employment of a variety of innovative techniques, which combined provide users with cm-level real time position accuracy anywhere on or near the earth's surface.

This new positioning technique is based on the generation and delivery of precise satellite corrections (i.e. orbit, clocks, and others) on a global scale, either through a satellite link or the internet. The innovative aspects of the new solution can be divided into different categories, which directly relate to the areas that have represented different levels of limitation on making global high accuracy positioning possible. These areas are:

- a) Integer level ambiguities derivation;
- b) Real-time, high accuracy satellite corrections generation;
- c) Data transmission optimization;
- d) Positioning technology.

During the following sections we will explore each of those areas, highlighting the new aspects of the solution, as well as pointing out differences with respect to existing technologies, some of which are available in commercial services. In that sense we will explain why, and how,

RTX is a solution different from both differential RTK and precise point positioning as currently understood by the general GNSS community.

SYSTEM OVERVIEW

The RTX technology is employed to offer cm-level GNSS positioning through the CENTERPOINT RTX™ service. The general infra-structure of the system can be in the schematic flowchart below.

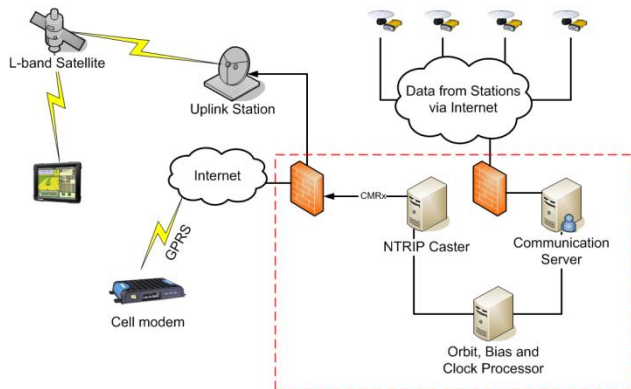


Figure 1. CENTERPOINT RTX™ infra-structure.

Data from monitoring stations distributed around the globe are collected and transmitted via the internet to

operation centers at different locations. The complete operation centers (encapsulated by the dashed red square in Figure 1) are redundant in order to assure the very high (~100%) availability of the system. In case it is needed, the correction stream source might change between operation centers and/or processing servers within centers. These operational changes are completely handled in a deterministic way by all parts of the system including the user receiver. Inside the operation centers redundant communication servers are used to relay the network observation data to the data processing servers, which host the network processors that produce precise orbit, clock, and observation biases valid for any place on the globe.

After being generated, the precise satellite data are compressed in messages compliant with the CMRx format, especially developed for compact transmission of satellite information. The messages are finally routed to either an uplink station or made available for internet connection access by the users.

The CENTERPOINT RTX™ tracking network is currently composed of around 100 stations, fairly well distributed across the globe. Figure 2 shows the location of stations used in the system.

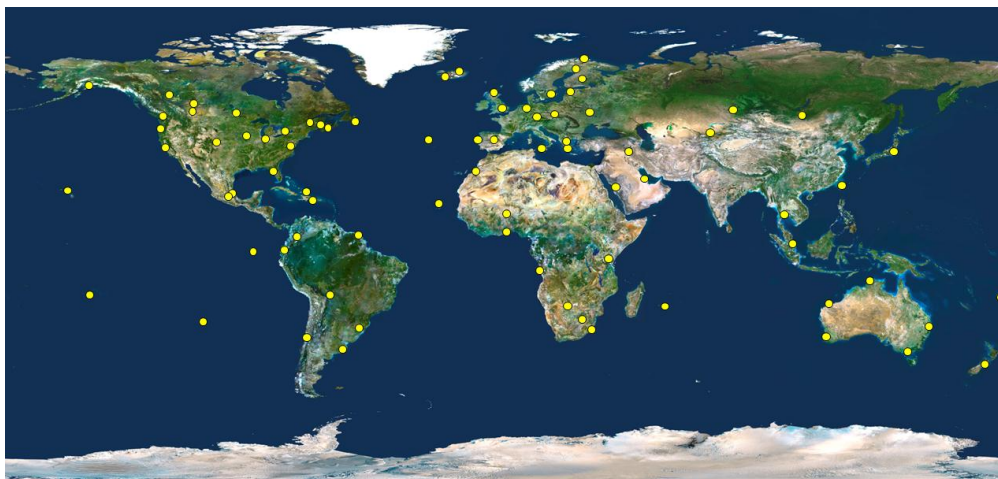


Figure 2. CENTERPOINT RTX™ tracking network distribution.

The CENTERPOINT RTX™ service is currently offered in the central region of North America, via satellite link, as indicated in Figure 3.

Since October 2011 the CENTERPOINT RTX™ service has been also offered to users in Australia. In this region the service is currently offered for users with access to internet connection (Figure 4).



Figure 3. CENTERPOINT RTX™ service coverage in Central North America.



Figure 4. CENTERPOINT RTX™ service coverage in Australia.

ABSOLUTE HIGH ACCURACY GNSS POSITIONING LIMITING FACTORS

In this section we will explore several aspects of absolute GNSS positioning in order to highlight what are the limiting factors in obtaining real time high accuracy positions from GNSS on a global scale. This introduction is convenient as it also highlights the innovation elements that have been necessary for creating the RTX global RTK system.

It is convenient to start from simplified basic GNSS observation equations:

$$\Phi_i = \rho + c(dT - dt) + T - I_i + \lambda_i N_i, \quad (1)$$

$$+ A_i - a_i + \frac{W_\Phi - w_\Phi}{\lambda_i} + B_{\Phi,i} - b_{\Phi,i} + M_{\Phi,i} + n_{\Phi,i}$$

and

$$P_i = \rho + c(dT - dt) + T + I_i, \quad (2)$$

$$+ A_i - a_i + B_{P,i} - b_{P,i} + M_{P,i} + n_{P,i}$$

where:

Φ_i is the carrier-phase measurement for frequency i in meters;

ρ is the geometric distance between the antennas of the receiver and satellite in meters;

c is the speed of light constant in meters per second;

dT is the receiver clock error in seconds;

dt is the satellite clock error in meters per second;

T is the slant neutral atmosphere delay in meters;

I_i is the ionospheric delay for frequency i in meters;

λ_i is the carrier-phase wavelength for frequency i in meters;

N_i is the integer carrier-phase ambiguity for frequency i in cycles;

A_i is the combined receiver antenna offset and directional variation correction for frequency i in meters;

a_i is the combined satellite antenna offset and directional variation correction for frequency i in meters;

W_Φ is the receiver antenna phase wind-up effect, in cycles;

w_Φ is the satellite antenna phase wind-up effect, in cycles;

$B_{\Phi,i}$ is the carrier-phase receiver bias for frequency i in meters;

$b_{\Phi,i}$ is the carrier-phase satellite bias for frequency i in meters;

$M_{\Phi,i}$ is the carrier-phase multipath for frequency i in meters;

$n_{\Phi,i}$ is the carrier-phase observation noise and other unmodeled effects for frequency i in meters;

P_i is the pseudorange measurement for frequency i in meters;

$B_{P,i}$ is the pseudorange receiver bias for frequency i in meters;

$b_{P,i}$ is the pseudorange satellite bias for frequency i in meters;

$M_{P,i}$ is the pseudorange multipath for frequency i in meters;

$n_{P,i}$ is the pseudorange observation noise and other unmodeled effects for frequency i in meters.

The feasibility of high-accuracy absolute positioning relies on the assumption that phase and code measurements on the different frequencies or on specific observation combinations are modeled quite reliably. This ultimately means that the parameters (or certain combination of them) of equations 1 and 2 are known very precisely, i.e., with an accuracy of better than a few centimeters.

Having a global system where every component of the un-differenced GNSS observational model is well known requires advanced understanding and modeling of the involved GNSS-related effects. This is a general achievement of the RTX system. Aspects of some of these

components including their importance for global positioning are now discussed.

Apart from the effects that are detailed below, there are a number of corrections that have also to be considered in order to achieve cm-level positions in a given earth-centered reference frame. Some of these effects are solid earth tides, ocean tidal loading, and polar motion. Details on how these effects can be modeled can be found in Petit and Luzum (2010).

Satellite orbits and clocks

The receiver coordinates, which are the parameters of most interest for us, primarily depend on the geometric distance, and thus hold a relationship with all other parameters belonging to the same observation equation. Some of those and their relevance for positioning are now explored.

The geometric range ρ in equations 1 and 2 can be represented as a traditional norm computation formula, thus:

$$\rho = \sqrt{(X_r - X^s)^2 + (Y_r - Y^s)^2 + (Z_r - Z^s)^2} \quad (3)$$

where:

X_r, Y_r, Z_r are coordinates of the receiver antenna reference point in the ECEF coordinate system at the time of signal reception, in meters;
 X^s, Y^s, Z^s are coordinates of the satellite center of mass in the ECEF coordinate system at the time of the signal transmission, in meters.

It is important to note that in a system such as RTX, where satellite clocks are computed using a given set of satellite orbits (in our case the RTX real-time orbits), certain components of the orbit errors are absorbed by the estimated clocks and have their impact on positioning minimized. The component of the orbital error that gets mostly minimized is somewhat near the direction of the radial component (generally pointing towards the earth). The exact direction of the minimum orbit error impact on positioning is not straight forward to be determined, as it depends on the network coverage and other aspects of the clock processing model such as observation weighting. However it is fair to say that the impact of the orbit error on positioning is dependent on the angle between the receiver-satellite line of sight (vector r in Figure 5) and the direction of minimum orbit error impact (vector e in Figure 5).

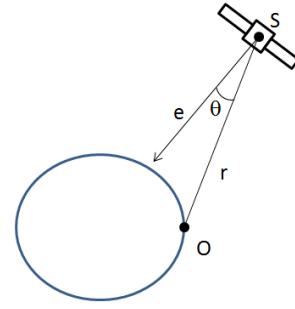


Figure 5. Satellite orbital error impact geometry

In order to assure high reliability in global positioning and global network data processing it is of fundamental importance that satellite orbital errors are minimal, since most of the other components of the system depend on the quality of this information.

Both satellite orbits and satellite clock errors (dt in equations 1 and 2) are considered as known by the positioning engine. This means that any error in the satellite clock provided by the network processing will translate directly into an observation modeling error of same magnitude.

Receiver clock error

The receiver clock error, dT in equations 1 and 2, is usually implemented as a parameter in positioning engines that employ an un-differenced observation model. In that case the parameter is normally modeled as a white noise process. In the case of (between satellites) differential observations, the receiver clock term is eliminated and does not need to be explicitly modeled.

In case of satellite systems operating with CDMA (*Code Division Multiple Access*), such as GPS, all satellites transmit their signals in the same frequency. Because of this the receiver-dependent carrier-phase and code biases are usually the same for all satellites. Thus it is possible to eliminate these terms with a between-satellite single-difference operation, or to assume that they are estimated as part of the receiver clock error. In the latter case equations 1 and 2 would read:

$$\begin{aligned} \Phi_i &= \rho + c(dT'_{\Phi,i} - dt) + T - I_i + \lambda_i N_i \\ &+ A_i - a_i + \frac{W_{\Phi} - w_{\Phi}}{\lambda_i} - b_{\Phi,i} + M_{\Phi,i} + n_{\Phi,i}, \end{aligned} \quad (4)$$

and

$$\begin{aligned} P_i &= \rho + c(dT'_{P,i} - dt) + T + I_i \\ &+ A_i - a_i - b_{P,i} + M_{P,i} + n_{P,i}, \end{aligned} \quad (5)$$

where

$$dT'_{\Phi,i} = dT + \frac{B_{\Phi,i}}{c}, \quad (6)$$

and

$$dT'_{p,i} = dT + \frac{B_{p,i}}{c}. \quad (7)$$

It is interesting to note that when making the assumption that the receiver biases can be modeled along with receiver clock parameters, the perceived clock error becomes inconsistent between phase and code measurements. In some cases this feature might play a role, and special procedures such as keeping a bias parameter for one of the two might have to be put in place. There have been efforts in using observation models using a decoupled phase-code clock approach applied to PPP techniques, such as in Collins et al. (2008).

In case of satellite systems employing FDMA (*Frequency Division Multiple Access*) signals, such as GLONASS, different satellites use different transmission frequencies. This is a limiting factor for positioning in general, but even more for global high-accuracy positioning. The fact that the assumption of bias absorption by the perceived receiver clock is no longer entirely valid introduces a burden on how the measurement biases for different satellites can be accounted for. The problem is even more critical when combining data collected with receivers from different manufacturers as the experienced biases might be significantly different for different receiver types.

Antenna phase center modeling

GNSS measurements refer to the antenna phase centers of receivers and satellites. Such antenna phase centers typically do not coincide with reference position points for neither satellite nor receiver. In case of the receiver it is usual to have the bottom of antenna mount as the reference point. For the satellite, positions typically refer to its center of mass. The offsets between these reference points and the antenna phase centers have to be accounted for, as these values can reach a couple of meters for the spacecraft, and can be at the decimeter level for receivers. In case of the satellites there is one additional complicating factor which is the required knowledge of the satellite attitude, since the antenna offsets are known for the satellite body coordinate system, and thus a transformation to the earth-centered coordinate system is required before accounting for this quantity in the measurement domain. The most challenging component of the satellite attitude is the yaw, as for some satellites the yaw maneuvering during and around eclipsing seasons is not completely deterministic.

In addition to the antenna offsets, variations on the phase center position for different observed azimuth and elevation (or nadir angle, in case of the satellite) have also to be taken into account. The antenna phase center variation effects are typically in the range of few mm. More details on standardized antenna correction can be found for example on Rothacher and Schmid (2010). Both

type of antenna corrections, offset and variation, shall be properly accounted for receiver and satellites in a global cm-level GNSS application.

Phase wind-up effects

The receiver antenna phase wind-up W_ϕ is of peculiar nature, since for some practical GNSS positioning applications there might be absolutely no model that can describe the expected wind-up effect due to the unpredictable nature of the antenna movements. It is important to note, however, that the phase wind-up component caused by rotation of the antenna along its axis (yaw) is common for all satellites in view. Rotation in the other directions (i.e., roll, pitch) results in phase wind-up effects that are different for each satellite, dependent on the geometry.

The satellite phase wind-up w_ϕ can be computed from models that describe the satellite attitude. There have been some efforts from the GNSS community in the direction of properly modeling the GNSS satellites attitude, especially concerning the yaw attitude of some satellite types such as GPS block IIA and GLONASS satellites (see e.g. Bar-Sever (1995), Kouba (2008), Dilssner et al. (2010)). If used, such models have to be carefully employed in order to avoid problems for high-accuracy observation modeling.

Neutral atmosphere delay

The neutral atmosphere (or troposphere, for simplicity) incorporates the delay suffered by the GNSS signal due to the presence of gases in the atmosphere, including water vapor. In the case of the troposphere, the relationship between the slant delay at a given elevation angle and the delay that would be experienced at the zenith direction is in general well known. This relationship is represented by tropospheric mapping functions, thus:

$$T = mf \cdot T^z, \quad (8)$$

where mf is the mapping function for the tropospheric delay, and T^z is the zenith delay. Furthermore, both the delay and the mapping function can be separated into two components, normally referred to as wet and hydrostatic (or dry). Equation 4 can then be re-written as:

$$T = mf_h \cdot T_h^z + mf_{nh} \cdot T_{nh}^z \quad (9)$$

In the case of real-time absolute positioning it is usual that the tropospheric delay is not well known. This is because atmospheric prediction models suitable for real-time receiver operation (such as UNB3, UNB3m, and GPT models – Collins and Langley (2007), Leandro et al. (2006), and Böhm et al. (2007), respectively) provide typical accuracies of up to a few decimeters at zenith direction (Collins et al. (1996), Leandro (2009)), with errors being mostly caused by the variability on the amount of water in the atmosphere for the region and time

of interest. The lack of reliable *a priori* information and a well understood relationship between slant and zenith delays makes the modeling of the tropospheric delay as a parameter the most suitable option for handling this effect in absolute high accuracy positioning. In this case the parameter estimated is typically the zenith delay or a variation of it, such as delay scaling factor.

The limitation in such an approach is the assumption that the mapping function is enough for describing the behavior of the delays. This assumption becomes invalid in cases where the slant delays do not have a symmetric behavior with respect to the receiver-satellite azimuthal direction. This typically occurs in the presence of weather fronts where the amount of water vapor in the atmosphere is changing more dramatically in certain directions than in others. The asymmetric behavior of the troposphere imposes a challenge for high accuracy, real-time global GNSS positioning.

Ionospheric delay

The ionospheric delay (I_i in equations 1 and 2) is one of the important limiting factors in global positioning. This is because information on the behavior of the ionosphere on a global scale is quite limited in terms of accuracy, even in post-processing products. The most reliable products available for the GNSS community are the IGS (*International GNSS Service*) ionospheric maps made available with latencies as short as one day after data collection. These maps have a usual accuracy of 2-8 TECUs (International GNSS Service (2011)). One TECU (Total Electron Content Unit) is equivalent to around 0.16 m delay for the L1 frequency, remembering that being a dispersive medium, the ionosphere causes different delays on different frequencies. As widely known, the ionospheric delay is inversely proportional to the squared signal frequency. The actual relationship reads:

$$I_i = \frac{40.3 \cdot TECU}{f_i^2}, \quad (10)$$

where f_i is the GNSS frequency i in MHz. It is therefore also easy to derive the relationship of the ionospheric delay between different frequencies:

$$I_i = \frac{f_j^2}{f_i^2} I_j, \quad (11)$$

where subscripts i and j stand for frequencies i and j , respectively. Another relationship caused by the dispersive nature of the ionosphere is the inverse impact it causes in carrier-phase and code measurements. While code measurements suffer a signal delay, carrier-phase measurements suffer an advance. Please note that in this text we are referring to the ionospheric terms as delays, and thus these terms are reduced in the carrier-phase measurement equations, while added in the pseudorange ones.

Even in the absence of accurate *a priori* information the handling of the ionosphere in positioning can take several forms, depending on the positioning engine setup and the targeted usage of the derived ionospheric information. For instance it is possible to handle the ionospheric delay as a parameter of the un-differenced GNSS observation model. In this case the iono delay is derived using the relationships established by equations 1, 2, 10, and 11, and thus one unique ionospheric delay parameter can be estimated with code and carrier-phase measurements from different frequencies.

Another way of handling the ionosphere is creating observation combinations from which the delay can be explicitly derived. These combinations are usually formed in a way to eliminate non-dispersive effects. This is the case for the ionospheric phase combination, where:

$$\Phi_{iono} = \Phi_i - \Phi_j \quad (12)$$

and therefore:

$$\begin{aligned} \Phi_{iono} &= \left(\frac{f_i^2}{f_j^2} - 1 \right) I_i + \lambda_i N_i - \lambda_j N_j \\ &+ \frac{(\lambda_j - \lambda_i) W_{\Phi} - W_{\Phi}}{\lambda_i \lambda_j} \\ &+ B_{\Phi,i} - B_{\Phi,j} - b_{\Phi,i} + b_{\Phi,j}, \end{aligned} \quad (13)$$

where Φ_{iono} is the ionospheric carrier-phase combination in meters. Multipath and noise terms have been neglected, and antenna corrections are assumed to be properly applied prior or after the observation combination. It is important to note that if the combination above is to be used for integer ambiguity derivation, the other outstanding parameters have to be precisely known, or also derived. This means a proper modeling and/or estimation of the receiver and satellite phase wind-up effects, and the ionospheric phase bias term, which can be represented as:

$$B_{\Phi,iono} = B_{\Phi,i} - B_{\Phi,j} - b_{\Phi,i} + b_{\Phi,j}, \quad (14)$$

and thus:

$$\begin{aligned} \Phi_{iono} &= \left(\frac{f_i^2}{f_j^2} - 1 \right) I_i + \lambda_i N_i - \lambda_j N_j \\ &+ \frac{(\lambda_j - \lambda_i) W_{\Phi} - W_{\Phi}}{\lambda_i \lambda_j} + B_{\Phi,iono}. \end{aligned} \quad (15)$$

Likewise the carrier-phase, the pseudorange measurements can also be used to form an ionospheric combination, as shown below.

$$P_{iono} = P_i - P_j = \left(1 - \frac{f_i^2}{f_j^2} \right) I_i + B_{P,iono}, \quad (16)$$

where:

$$B_{P,iono} = B_{P,i} - B_{P,j} - b_{P,i} + b_{P,j}. \quad (17)$$

Another very common way of handling the ionospheric delay present in the measurements is by combining them in a way that the delay gets eliminated. In fact only the first order of the ionospheric delay (as represented in equation 10) is differenced out, and second and higher order components of the ionosphere might still be present in the ionospheric-free combination afterwards. The second order component typically represents delays at mm to cm level for L1 frequency (Morton et al. (2009)), and in most real time applications are neglected.

The first variation of ionospheric-free combination we will discuss is the combination between two frequencies of carrier, yielding into an iono-free phase measurement, or code, which yields into the iono-free code measurements. The ionospheric-free carrier phase measurement can be formed as follows:

$$\Phi_{if,i,j} = \frac{f_i^2}{f_i^2 - f_j^2} \Phi_i - \frac{f_j^2}{f_i^2 - f_j^2} \Phi_j, \quad (18)$$

and thus:

$$\begin{aligned} \Phi_{if,i,j} &= \rho + c(dT - dt) + T + \lambda_{if,i,j} N_{if,i,j} \\ &+ \frac{W_\Phi - w_\Phi}{\lambda_{if,i,j}} + B_{\Phi,if,i,j} - b_{\Phi,if,i,j} \\ &+ M_{\Phi,if,i,j} + n_{\Phi,if,i,j}, \end{aligned} \quad (19)$$

where the antenna effects are assumed to be properly corrected; $\Phi_{if,i,j}$ is the ionospheric-free carrier phase combination formed with measurements from frequencies i and j - the same applies to all other terms with same subscript. This combination has not only been widely used in traditional GNSS, but it has also been established as a standard for applications where traditional precise absolute positioning is performed. The reason that makes this combination so important is the fact that it provides an observation that directly relates to the geometric components of the positioning model (e.g. the receiver coordinates) with no influence of the ionospheric delay, using an observation which has a reasonably low noise, especially if compared to code noise.

If one intends to derive integer level ambiguities in absolute positioning using the iono-free carrier-phase combination it is necessary that the phase wind-up for receiver and satellite antennas are properly modeled or corrected. Furthermore, assuming an approach where the receiver phase bias will be modeled along with the receiver clock (e.g. equations 4 and 6) or eliminated by differencing observations between satellites, it becomes evident that the satellite phase bias term $b_{\Phi,if,i,j}$ has to be accounted for. As it would be difficult to model this bias as an additional parameter in a single-receiver positioning

processor, these values, or a combination of values from each these can be derived, have to be ideally provided by the network processors. This is the case for the RTX system.

The ionospheric-free pseudorange can be derived in a similar manner as the carrier-phase:

$$P_{if,i,j} = \frac{f_i^2}{f_i^2 - f_j^2} P_i - \frac{f_j^2}{f_i^2 - f_j^2} P_j, \quad (20)$$

and thus:

$$\begin{aligned} P_{if,i,j} &= \rho + c(dT - dt) + T \\ &+ B_{P,if,i,j} - b_{P,if,i,j} \\ &+ M_{P,if,i,j} + n_{P,if,i,j}, \end{aligned} \quad (21)$$

Pseudorange are commonly used in positioning solutions for a number of different reasons. Besides the fact that pseudorange observables are often used for computation of the signal transmission time, their un-ambiguous nature makes these measurements a powerful component in GNSS positioning, for both rover positioning and network processing. It is important to note that if iono-free code measurements are used, observation biases with respect to phase of same combination might have to be accounted for. In addition to the satellite observation bias $b_{P,if,i,j}$ which follows the same logic as for the respective term of the carrier-phase measurement, it might also be necessary to account for receiver biases between code and phase, which in this case can be written as:

$$B_{\Phi-P,if,i,j} = B_{\Phi,if,i,j} - B_{P,if,i,j}. \quad (22)$$

The other possible approach to account for the code-phase bias inconsistency is to directly model the perceived clocks for code and phase measurements ($dT'_{\Phi,i}$ and $dT'_{P,i}$) separately.

Ionospheric-free combinations can also be formed combining code and phase measurements. This can be done in different ways, and each combination can be employed for different purposes in positioning and network processing algorithms. One peculiar code-carrier combination is between the narrow-lane code, and wide-lane phase. Differencing these two combinations yields an ionospheric-free and geometry-free measurement. The wide-lane phase can be obtained as:

$$\Phi_{wl,i,j} = \frac{f_i}{f_i - f_j} \Phi_i - \frac{f_j}{f_i - f_j} \Phi_j, \quad (23)$$

and thus:

$$\begin{aligned} \Phi_{wl,i,j} &= \rho + c(dT - dt) + T + \frac{f_i}{f_j} I_i + \lambda_{wl,i,j} N_{wl,i,j} \\ &+ B_{\Phi,wl,i,j} - b_{\Phi,wl,i,j} + M_{\Phi,wl,i,j} + n_{\Phi,wl,i,j}. \end{aligned} \quad (24)$$

Please note that phase wind-up effects are cancelled out in the wide-lane phase combination, and that the ionospheric delay has its sign inverted. The narrow-lane code observation can be created as:

$$P_{nl,i,j} = \frac{f_i}{f_i+f_j} P_i + \frac{f_j}{f_i+f_j} P_j, \quad (25)$$

and thus:

$$P_{nl,i,j} = \rho + c(dT - dt) + T + \frac{f_i}{f_j} I_i + B_{P,nl,i,j} - b_{P,nl,i,j} + M_{P,nl,i,j} + n_{P,nl,i,j}. \quad (26)$$

Since the ionospheric delay assumes the same form for both wide-lane phase and narrow-lane code, differencing these two combinations results in an ionospheric-free measurement. Furthermore, the geometric effects (geometric distance, clocks, troposphere) are also cancelled out. Therefore, this combination provides a direct measure of the wide-lane combination of carrier-phase ambiguities, along with the respective code and phase measurement biases, multipath and noise:

$$\begin{aligned} \Phi_{wl,i,j} - P_{nl,i,j} &= \lambda_{wl,i,j} N_{wl,i,j} \\ + B_{\Phi,wl,i,j} - b_{\Phi,wl,i,j} + M_{\Phi,wl,i,j} + n_{\Phi,wl,i,j} \\ - B_{P,nl,i,j} + b_{P,nl,i,j} - M_{P,nl,i,j} - n_{P,nl,i,j} \end{aligned} \quad (27)$$

The narrow-lane code and wide-lane phase combination has been introduced by Garbor and Nerem (2002) as a means of resolving ambiguities for global positioning. After that a number of authors have adopted and refined this approach. The power of this combination is the detachment of the ambiguity parameter from the geometric terms, as previously pointed out. As a drawback, the code noise and code and phase bias parameters have to be properly handled. There are other code and carrier combinations that provide similar benefits. This is the case for combinations between code measurements of a particular frequency and carrier-phase measurements from two frequencies. The phase data can be combined in a specific way to cancel out geometric and ionospheric effects of pseudoranges observed on a given frequency, say, frequency i , as derived below. In this text we are calling this combination as *divergence-free* phase combination and it can be formulated as follows:

$$\Phi_{df,i} = \frac{f_i^2 + f_j^2}{f_i^2 - f_j^2} \Phi_i - \frac{2f_j^2}{f_i^2 - f_j^2} \Phi_j, \quad (28)$$

and thus:

$$\begin{aligned} \Phi_{df,i} &= \rho + c(dT - dt) + T + I_i + \lambda_{df,i} N_{df,i} \\ + B_{\Phi,df,i} - b_{\Phi,df,i} + M_{\Phi,df,i} + n_{\Phi,df,i}. \end{aligned} \quad (29)$$

The divergence-free phase can then be combined with the code measurement:

$$\begin{aligned} \Phi_{df,i} - P_i &= \lambda_{df,i} N_{df,i} \\ + B_{\Phi,df,i} - b_{\Phi,df,i} + M_{\Phi,df,i} + n_{\Phi,df,i} \\ - B_{P,i} + b_{P,i} - M_{P,i} - n_{P,i} \end{aligned} \quad (30)$$

While this combination provides the possibility of working with code measurements obtained on one single frequency, the wavelengths obtained for the divergence-free carrier-phase ambiguities are very short. As a reminder, for all cases of code and carrier combinations above the resulting biases for both, or combined, carrier and code measurements have to be properly accounted for in ambiguity resolution-enabled GNSS processing.

REAL-TIME NETWORK PROCESSING

As mentioned earlier, the RTX system works based on precise satellite information which is generated at processing centers, and broadcast to users. The precise information employed by the systems comprises satellite orbits, satellite clocks, satellite biases, and other auxiliary information. In this section we will explore aspects of each of those components.

The requirements for the satellite orbits to be used in the global RTX system can be summarized as accuracy, continuity, robustness and reliability. The satellite positions have to be accurate for obvious reasons, including the fact that orbit errors have direct impact on rover position determination quality. Furthermore, because the RTX network process algorithms use ambiguity resolution, the reliability of the ambiguity determination is highly affected by the satellite orbits quality due to the distances between reference stations in the tracking network. The continuity requirement is put in place to avoid the need of handling observation modeling inconsistency over time for both network and rover processing. For the same reason the overall system employs techniques to properly handle switches between redundant orbit processing servers without degradation of position quality. As one would expect, network processors have to be in general robust against the eventuality of poor data entering the system for various reasons. The RTX network processors employ a variety of quality control techniques to ensure that only data with the highest expected quality is used for the computation of end products. Last but not least, the reliability is a very important factor for real-time orbit processing. At the current stage the RTX real-time orbit processors are able to run for several months with virtually zero intervention from operators, while handling events such as satellites going through unhealthy periods and satellite maneuvers (during unhealthy period or not).

There are at least two strong reasons for justifying the need of implementing and running an RTX proprietary

orbit processing server. The first one is simply the need of reliably meeting the above mentioned requirements. The second one is that from an operational perspective, the RTX system is conceived in such a way that it does not rely on any external source of information to be able to run at its full accuracy capability. In Figure 6 it is possible to see the achieved orbit errors provided by IGS ultra-rapid products during two weeks of March 2011, where

IGS rapid orbit products are used as truth. The ultra-rapid orbits are evaluated using the initial portion of the predicted arc, thus making use of the most reliable part of the predicted arcs as the products become available in real-time. In that case neither accuracy nor continuity requirements for RTX processing are completely met.

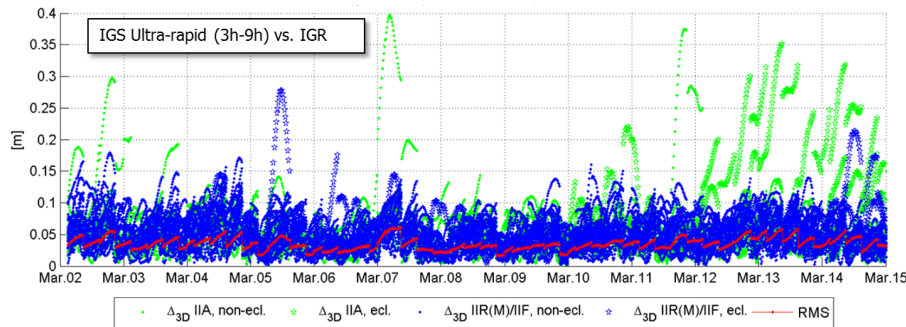


Figure 6. IGS ultra-rapid orbit errors, as compared to IGS rapid orbit products.

The orbit estimation in the CENTERPOINT RTX™ system is based on a combination of a UD-factorized Kalman filter estimating satellite position, satellite velocity, troposphere states, integer ambiguities, solar radiation pressure parameters, harmonic coefficients, and earth orientation parameters. The prediction step in the filter is using a numerical integration of the equations of motion in connection with a dynamic force modeling. The basic principles of the approach are described by Landau (1988). Forces considered in the approach are

- The earth's gravity field
- Lunar and solar direct tides
- Solar radiation pressure
- Solid earth tides
- Ocean Tides
- General Relativity

In RTX orbit processing carrier phase integer ambiguities are resolved in real-time. Also, the satellite orbit states are truly estimated in real-time and continuously adapted over time to better represent the current reality. This means that the satellite positions that are evaluated by the user have prediction times of no more than a few minutes since the last orbit processing filtering update, providing negligible loss of accuracy. In Figure 7 the orbit errors obtained from the RTX orbit processor can be seen. Similarly to the previous figure, IGS rapid orbit products are used as reference. The time span is also the same as in the previous figure. The RTX real-time orbit components have a typical overall accuracy of around 2.5 cm, and a 3D error accuracy of around 4 cm, considering IGS rapid products as truth.

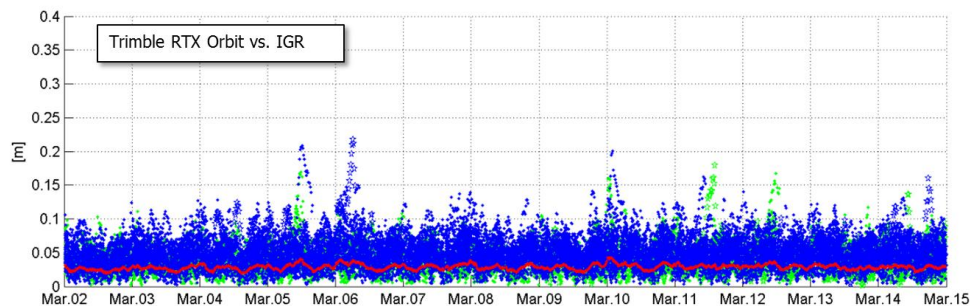


Figure 7. RTX real-time orbit errors, as compared to IGS rapid orbit products.

Satellite clock estimation is an essential part of the RTX system. It plays a fundamental role on positioning performance due to a number of reasons. Satellite clocks map directly into line-of-sight observation modeling, yielding into a one to one error impact from clocks into

GNSS observables modeling. Due to the same strong relationship, it is of fundamental importance that clocks are generated in a way to facilitate ambiguity resolution within the positioning engine. The processing speed of a clock processor is also of fundamental importance, due to

the fact that any delay in computing satellite clocks is directly translated into correction latencies when computing real-time positions on the rover side. For that matter one should keep in mind that regardless how late satellite corrections get to the GNSS receiver in the field, positions have to be provided to the user as soon as the rover GNSS measurements are available. Therefore latencies typically introduce errors into the final real time position. In this paper we define real-time positioning as the computation of positions at the time when the rover observables are available, regardless the latency of the correction stream. This is a necessary concept in order to support dynamic rover GNSS positioning.

The RTX clock network processor was designed around the requirements discussed above. It computes clocks that are compatible with ambiguity resolution on the user receiver. As a matter of fact, the clock network processor itself employs ambiguity resolution for the generation of the RTX clocks. The processor architecture is based on an innovative design which allows processing data of several hundreds of reference stations, including all necessary steps such as data quality control, ambiguity resolution, and the final clock generation, within a fraction of second. The processing time of this kind of real time network processor has to be minimized as much as possible in order to allow the processor to operate at 1 Hz, and to minimize the final correction latency at the rover end. It is important to note that the final latency of the correction stream is a composition of three basic components: the time for the network data to arrive at the network processing server; the network processing time; and the correction transmission time to reach the final user. Figure 8 shows the typical total correction latency for the RTX system, when corrections are broadcast through a satellite link.

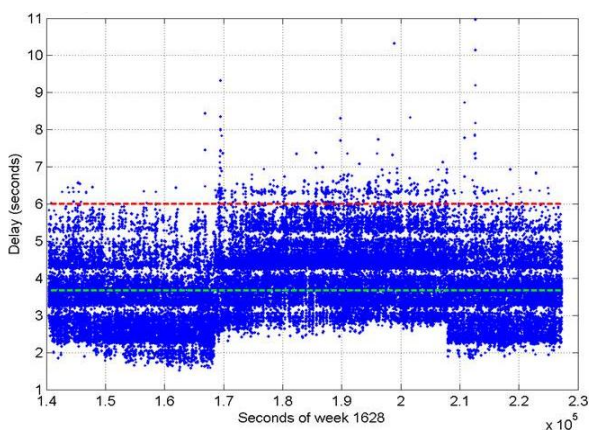


Figure 8. Typical RTX correction stream latency. The dashed green line represents the latency at 50% (3.7 s), and the dashed red line represents the latency at 99% (5.6 s.)

Unlike satellite orbits, satellite clock solutions are more difficult to be directly compared. This is because different clock solutions might have offsets between each other, as well as behave differently due to differences in their GNSS reference time realization process as well as in

their observation modeling approaches. That said, one way of verifying the quality of satellite clocks is to quantify how well it can be used to model actual receiver observation data. This can be in general achieved by applying satellite orbit and clock correction onto GNSS data and verifying the remaining residuals. Other quantities such as receiver coordinates have to hold their correct values for the residuals to be meaningful. One remark to be made concerning this type of assessment is that in this case not only the satellite clock quality is assessed, but the combined satellite orbit and clock error. For our purposes this is perfectly fine, since this is the way orbits and clocks are employed in rover positioning as well. Figures 9 and 10 show typical combined satellite orbit and clock errors at line of sight for different satellites. Figure 9 shows the ionospheric-free phase modeling error for GPS satellites, while Figure 10 is for GLONASS. Please note that observations of a reference satellite (highest elevation at the time of observation) were reduced from the others. This was done in order to remove the receiver clock errors from the residuals. As it can be seen, for both GPS and GLONASS cases the observation modeling error after using RTX orbit and clock corrections is on average at 1 cm level, with values typically less than 2 cm. The GPS satellite with outlying behavior in the plot below was setting at that time, and the increased amplitude of the residuals is mostly due to receiver observation errors such as multipath.

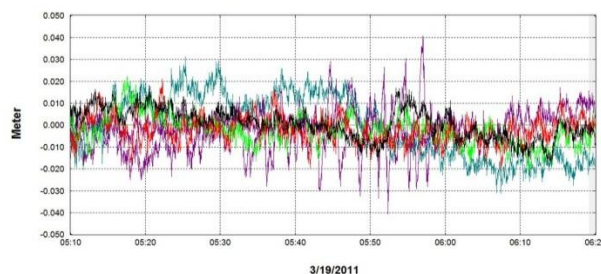


Figure 9. RTX clock quality (GPS) by means of corrected ionospheric-free phase measurements.

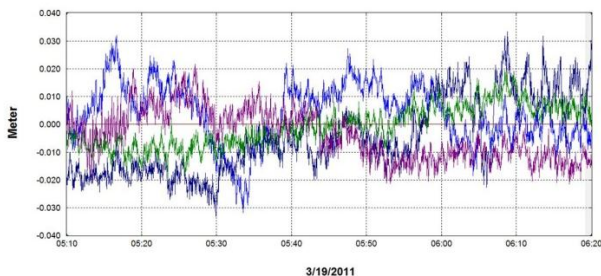


Figure 10. RTX clock quality (GLONASS) by means of corrected ionospheric-free phase measurements.

In addition to satellite orbits and clocks, satellite system biases are also of interest for high accuracy global GNSS positioning. As previously discussed, properly modeling observation biases is one of the requirements for achieving complete, accurate, cm-level global observation modeling in GNSS. This is the case because observation biases have to be either modeled or eliminated in order to

allow other parameters, such as position and ambiguities, to be accurately determined. Examples of observation biases are shown in most equations of this text. One remark to be made is that even though we are refereeing to these quantities as biases in this text, one should not assume that these offsets are necessarily constant, or stable, over time. In Figure 11 biases between two combinations of observations on L1 and L2 frequencies are shown for different satellites for June 2009. Values are quite stable over time for PRN 02, PRN 11 and PRN 19. The line for PRN 32 shows a case where biases slowly drift over time, which is not too uncommon. Further down in the plot the behavior for PRN 25 is shown. In this case not only the bias was slowly drifting until around the 17th day of June, but it also quickly changed level around that time. The satellite was healthy during this change. A few days later around June 26th the satellite was set unhealthy, thus no continuation on the estimated bias line. These examples show the importance of real time estimation and monitoring of satellite system biases, since the use of pre-established values would eventually fail in the occurrence of events such as a level change, or gradually degrade the performance in case of slow drifts. As mentioned earlier, satellite observation bias real-time estimation and monitoring is one of the components of the RTX system. The RTX network processing servers run bias network processors for this purpose.

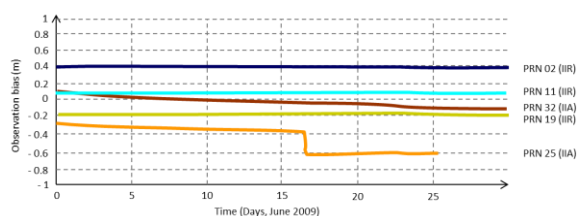


Figure 11. Satellite observation bias examples from June 2009.

COMMUNICATION AND POSITIONING

Once all satellite information is available, it has to be compressed in a message that can be broadcast to the user in the field. The transmission of global corrections can be done via internet, in case the user has access to it, or using a satellite link. In the later it is usual that corrections sufficient to cover the transmission satellite footprint are broadcast rather than corrections complete enough to cover the globe. Firstly, because it is expected that users operating inside the footprint of the satellite will be using the correction only for that region, and not anywhere else; secondly because bandwidth restrictions usually play a role in message design for satellite-based communication. The bandwidth restrictions do not only enforce that the maximum bandwidth utilization is below a certain limit, but also require that the utilization over time is homogeneous to ensure optimal usage of the satellite channel. Furthermore, satellite signals are typically susceptible to frequent message packet losses depending on the user environment, such as when a receiver is running under canopy. For mitigating the packet losses

the message has to be built in a way to allow the rover to continue to operate with minimum loss of availability. In that case not only the message design has to foresee this type of situation, but also the message decoding, usage and positioning algorithms have to be optimized to most favorably couple with the received messages. All these factors have been taken into account during the RTX system communication design. A new message format was created to carry information on satellite orbits, clocks, observation biases, and other auxiliary information. This new format was based on pre-existing concepts developed by Trimble as part of its RTK CMRx format. Among other aspects, the new RTX CMRx satellite messages:

- are independent from broadcast IODEs. The user is not required to couple the satellite messages with broadcast information restricted to a given IODE;
- have negligible inter-dependency. The messages are generally decodable irrespective of which messages have been received immediately prior to them. This characteristic differs from message designs using “delta” approaches, where information from (quasi-) consecutive messages has to be combined;
- deliver 1 mm resolution for satellite orbits and clocks, with clocks currently configured to be delivered at 2 seconds rate for satellite links, and 1 Hertz for internet links;
- have a bandwidth utilization (with 2 second clocks) of around 600 bps for covering the Americas, and 1200 bps for global coverage.

The RTX positioning engine inherits several technological aspects from Trimble’s pre-existent RTK engine. This aspect makes the RTX positioning mode, and traditional RTK positioning modes (e.g. single base, VRS) easy to co-exist. Among other things, the new engine has been thoroughly tested and optimized for challenging tracking environments. In these scenarios the engine is presented with observation data collected with a high level of multipath and low signal to noise ratio, often resulting in cycle slips and gaps in the data. As previously mentioned, at the same time the correction stream also suffers packet losses and the correction data might not be completely available during certain masking conditions.

As for positioning performance, the RTX engine delivers typical final accuracies at 1-2 cm level for horizontal positioning, and 2-4 cm for vertical. The final convergence of the system is achieved in 10 to 45 minutes after receiver startup. The time to converge might depend on several aspects, including satellite geometry and multipath conditions.

In order to overcome the increased convergence time as compared to traditional RTK systems, a number of features have been implemented as part of the RTX positioning engine, two of which are worthy of mention

here. The *Fast Restart* feature allows users who have not moved their equipment since the last RTX solution to power up the receiver – after any amount of time – and immediately obtain a converged solution. This feature is quite valuable, for example in Agriculture applications, where the user typically does not move his tractor between RTX-steered field work activities, avoiding for the majority of the time the need of waiting for new convergence period before start working one or more days after the last system usage. The second feature to be mentioned is also related to avoiding system re-convergence. A novel outage recovery capability makes the RTX positioning engine able to immediately recover from a complete constellation outage with loss of lock during any dynamic activity. This *Bridging* feature prevents the system from entering into a new convergence phase in case the receiver loses track of up to all satellites in view, coupled with outages of up to a couple of minutes, such as when running behind a tree line, or under a bridge.

POSITIONING PERFORMANCE

As mentioned earlier, the RTX system provides horizontal accuracies of around 1-2 cm, 1-sigma. Figure 12 shows an example of horizontal position error obtained in real time in a receiver acquiring the RTX correction data through the satellite link in North America. The receiver was running continuously for several days, and was located in Ames, Iowa, United States. As it can be seen in that example the horizontal RMS was 1.4 cm, with a 95% horizontal error of 2.4 cm. These are typical values for the satellite-based RTX horizontal performance.

Figure 13 shows the vertical performance for the same receiver and time period. As it can be seen the vertical RMS was 2.8 cm, with 95% vertical error of 4.4 cm.

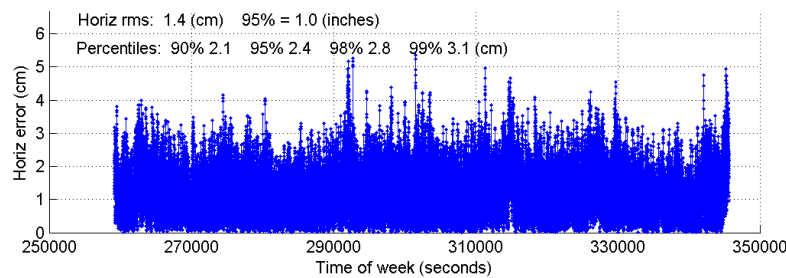


Figure 12. RTX real-time horizontal positioning performance. Results obtained from a receiver operating in Ames, Iowa, US.

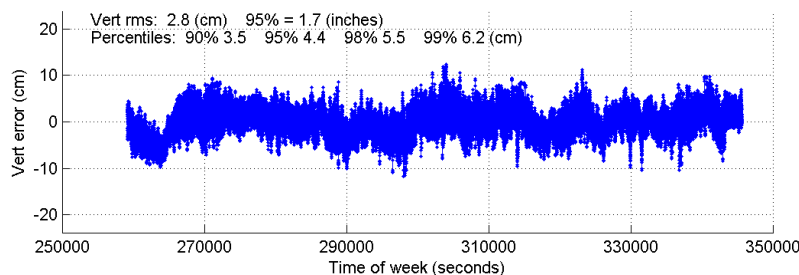


Figure 13. RTX real-time vertical positioning performance. Results obtained from a receiver operating in AMES, Iowa, US.

Another aspect of fundamental importance for the RTX system is the time to achieve convergence. This is important because convergence is directly connected to the level of productivity that can be achieved for actual field applications. In the example to follow a continuously powered RTX receiver was used in order to show an assessment of the RTX (re-) convergence capability. The receiver had tracking of all satellites disabled every hour

with an antenna switch. The duration of the outages were three minutes during which times no GNSS satellites were tracked. When the satellites are tracked again after the outages, all of them come back with cycle slips, as it can be seen in the outage phase tracking plot example in Figure 14. The colored lines indicate the tracked L1 phase of each satellite available at that time, and the black marks indicate cycle slips flagged in the phase data.

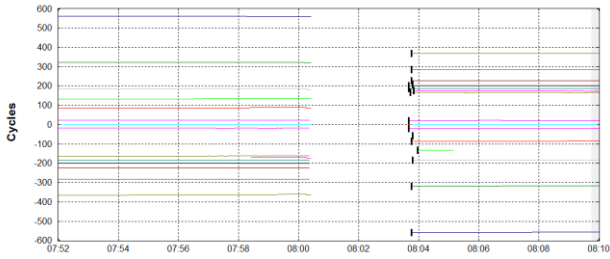


Figure 14. Phase tracking example for the induced data outages used in the re-convergence test.

This procedure is repeated hourly for several days in order to gather enough performance runs to derive meaningful statistics. Figure 15 shows the resulting performance of this type of assessment using the RTX system. Note carefully that the standard cold-start re-convergence performance is indicated with the blue lines, where the solid lines represent the 90% performance and the dashed line represents the 68% performance.

As it can be seen in Figure 15, the RTX system converged to better than 5 cm horizontal error after 20 and 25 minutes for 68% and 90% of the runs, respectively. One should keep in mind that the convergence time is correlated with a number of aspects, including the satellite geometry and multipath environment. Because of these variations the claimed convergence time for the RTX system is between 10 and 45 minutes for full accuracy achievement.

Yet in the plot below, the red lines indicate the performance obtained with a second receiver, connected to the same antenna, and thus subject to the exactly same GNSS signal outages. This second receiver had the *Bridging* functionality enabled, and thus is expected to bridge the outages and phase cycle slips without resetting the positioning solution.

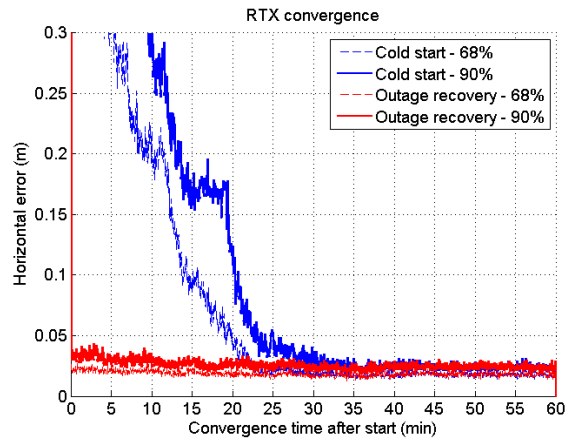


Figure 15. RTX re-convergence performance results.

The red lines in the plot above confirm the desired behavior is achieved. In order to better visualize what happens over time in this case, Figure 16 shows a few hours of the real-time results obtained with the receiver running with the *Bridging* functionality activated.

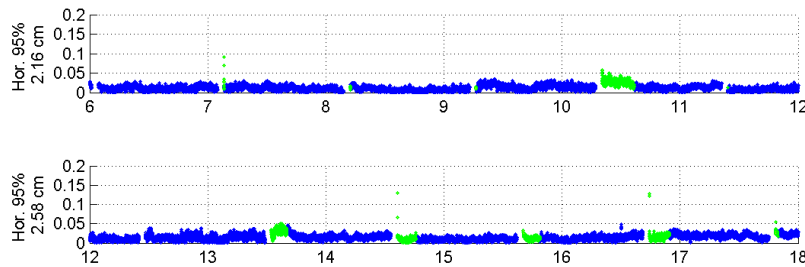


Figure 16. RTX outage recovery real-time performance.

In the next plot (Figure 17) an example of IP-based RTX performance is shown. This is a single run where the system converged to better than 5 cm (horizontal) in around 15 minutes. The interesting aspect to be explored in this dataset is the convergence of the ambiguities during the position processing. Figure 18 shows how the L1 ambiguities of individual satellites in view during that time converged.

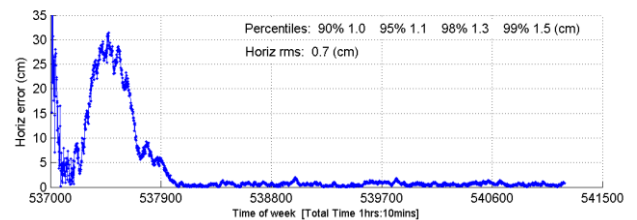


Figure 17. RTX IP-based run example.

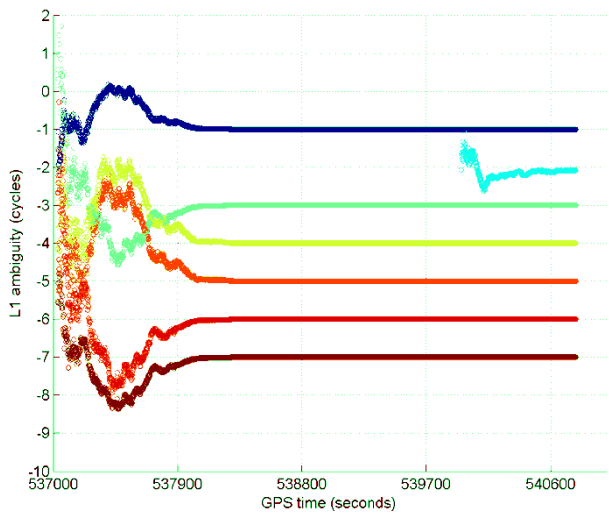


Figure 18. Example of ambiguities convergence during an RTX IP-based run.

As it can be noticed from the two plots above, the positioning convergence is, as expected, highly correlated with the ambiguities convergence to their final integer values in cycles. Also note that satellites that come in after the overall solution is converged (e.g. in light blue) achieve their final ambiguity values much quicker than during the position convergence phase, also as expected. Another consideration is that the proprietary algorithms used for ambiguity resolution and validation in RTX and other Trimble high precision GNSS positioning products allow the ambiguities to reliably converge to their integer values. Arbitrary integer number of cycles has been removed from the original ambiguity values to allow better simultaneous visualization of the ambiguities for several satellites.

As it was previously mentioned, the RTX positioning system has been optimized to work under different scenarios. This is necessary because the multipath and signal availability levels are reasonably different between running an antenna with a reference station setup, and the actual user environment, where the data tracking conditions impose additional challenges on making high accuracy positioning effective on a global basis, in a productive manner. Therefore, an extensive field test campaign was conducted during the pre-release phase of the RTX system. The next example shows RTX in-field performance for an Agriculture application in Illinois, US. The setup is typical for agricultural use, with the antenna and receiver mounted on a tractor that ran for around 103 minutes. The actual track of the tractor is shown in Figure 19. The RTX corrections were received via satellite link.



Figure 19. RTX tractor field test track in Illinois, US.

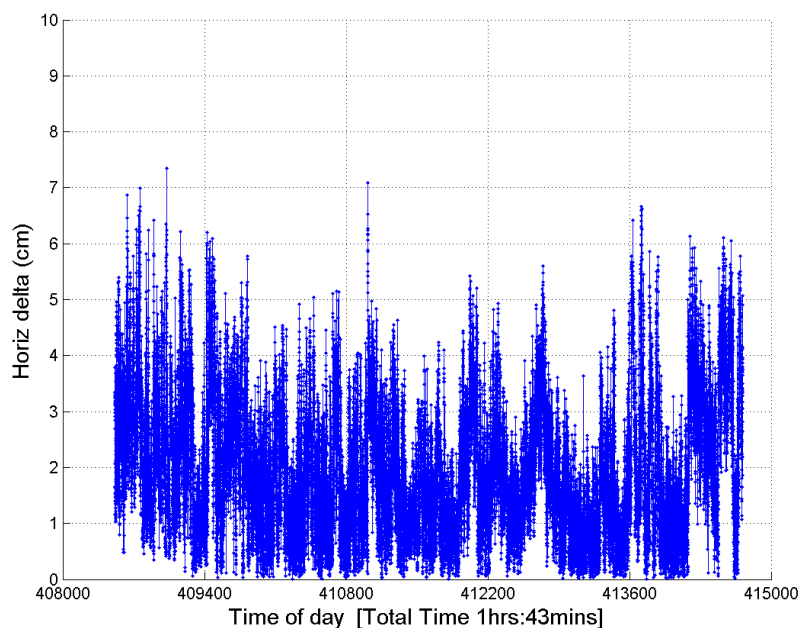


Figure 20. Horizontal positioning results for a real-time RTX tractor field test in Illinois, US.

The horizontal positioning performance for that field test can be seen Figure 20. The overall 2D RMS was 2.3 cm and the 95% horizontal error was 4.2 cm. Please note that this *position difference* plot is between the RTX solution and a short range single baseline (SBL) RTK solution providing ‘truth’. Therefore the numbers and plot above actually show a combination of errors between the global RTX solution and the SBL solution to the local reference station. Nevertheless the error magnitudes achieved are in the same range as in the previous assessments shown here.

CONCLUSIONS

RTX positioning is a new positioning technology that brings together the advantages of positioning techniques that do not require local reference stations while providing the productivity of RTK positioning. The deployment of the new system introduces innovations in GNSS network processing, as well as advancements in the rover global positioning algorithms.

The RTX solution employs ambiguity resolution on a global scale for both network and rover processing, including GPS and GLONASS satellites in the solution.

The delivery of this new technology is achieved through the positioning service CENTERPOINT RTX™, which is capable of providing world-wide real-time cm-level accuracy without the direct use of a reference station infrastructure.

REFERENCES

- Bar-Sever, Y.E. (1995). “A New Model for Yaw Attitude of Global Positioning System Satellites”. TDA Progress Report 42-123, November 15, 1995.
- Böhm, J., R. Heinkelmann, and H. Schuh (2007). “Short Note: A Global Model of Pressure and Temperature for Geodetic Applications”. *Journal of Geodesy*, doi:10.1007/s00190-007-0135-3, 2007.
- Collins P., F. Lahaye, P. Heroux, and S. Bisnath (2008). “Precise Point Positioning with Ambiguity Resolution using the Decoupled Clock Model”. *Proceedings of the 21st International Technical Meeting of the Satellite Division of The Institute of Navigation (ION GNSS 2008)*.
- Collins, P., and R. Langley (1997). “A Tropospheric Delay Model for the User of the Wide Area Augmentation System”. Final contract report for Nav Canada Satellite Navigation Program Office and published as Department of Geodesy and Geomatics Engineering Technical Report No. 187, University of New Brunswick, Fredericton, New Brunswick, Canada, September 1997.
- Collins, P., R. Langley, and J. LaMance (1996). “Limiting Factors in Tropospheric Propagation Delay Error Modelling for GPS Airborne Navigation.”. *Proceedings of The Institute of Navigation 52nd Annual Meeting*, Cambridge, Massachusetts, June 19-21 1996, pp. 519-528.
- Dilssner, F., T. Springer, G. Gienger, and J. Dow (2010). “The GLONASS-M satellite yaw-attitude model”. *Advances in Space Research*, Volume 27, Issue 1, 4 January 2011, Pages 160-171. doi:10.1016/j.asr.2010.09.007
- Garbor, M.J. and R.S. Nerem (2002). “Satellite-Satellite Single-Difference Phase Bias Calibration as Applied to Ambiguity Resolution”. *Journal of the Institute of Navigation*, Vol. 49, No. 4, pp. 223-242.
- International GNSS Service (2011). “IGS Products”. Web page available at <http://igsceb.jpl.nasa.gov/components/prods.html>. Accessed on October 1st 2011.
- Kouba, J. (2008). “A simplified yaw-attitude model for eclipsing GPS satellites”. *GPS Solutions*, Volume 13, Number 1, 1-12, DOI: 10.1007/s10291-008-0092-1
- Landau, H. (1988). “Zur Nutzung des Global Positioning Systems in Geodäsie und Geodynamik: Modellbildung, Software-Entwicklung und Analyse”, Heft 36 der Schriftenreihe des Studiengangs Vermessungs-wesen der Universität der Bundeswehr München, Dezember 1988
- Leandro, R. F. (2009). “Precise Point Positioning with GPS: A New Approach for Positioning, Atmospheric Studies, and Signal Analysis”. Ph.D. dissertation, Department of Geodesy and Geomatics Engineering, Technical Report No. 267, University of New Brunswick, Fredericton, New Brunswick, Canada, 232 pp.
- Leandro R.F., M.C. Santos, and R.B. Langley (2006). “UNB Neutral Atmosphere Models: Development and Performance”. *Proceedings of ION NTM 2006, the 2006 National Technical Meeting of The Institute of Navigation*, Monterey, California, 18-20 January 2006; pp. 564-573.
- Morton, Y. T., Q. Zhou, and F. van Graas (2009). “Assessment of second-order ionosphere error in GPS range observables using Arecibo incoherent scatter radar measurements”. *Radio Science*, Vol. 44, RS1002, doi:10.1029/2008RS003888.
- Petit, G., and B. Luzum (2010). “IERS Conventions (2010)”. *IERS Technical Note 36*, Frankfurt am Main: Verlag des Bundesamts für Kartographie und Geodäsie, 2010. 179 pp.

Rothacher, M., and R. Schmid (2010). "ANTEX: The Antenna Exchange Format, Version 1.4". Document available on-line at the International GNSS Service ftp server:
<ftp://igscb.jpl.nasa.gov/pub/station/general/antex14.txt>.